Experimental and Finite Element Modeling of Vinyl Ester Nanocomposites Under Blast and Quasi-Static Flexural Loading

Ahmad Almagableh,[1] P. Raju Mantena[2]

[1]*Al-Balqa Applied University, Faculty of Engineering Technology, Mechanical Engineering, Amman 11134, Jordan*
[2]*Composite Structures and Nano-Engineering Research Group, Mechanical Engineering Department, The University of Mississippi, University, Mississippi 38677*

Received 18 August 2011; accepted 26 January 2012
DOI 10.1002/app.36897
Published online in Wiley Online Library (wileyonlinelibrary.com).

ABSTRACT: Materials used in blast, penetration, and impact loaded structural applications require high strength and toughness under high strain rate loading. 510A-40 brominated bisphenol-A-based vinyl ester resin was developed and reinforced with different loadings of nanoclay and exfoliated graphite platelet to produce composites with optimal flexural rigidity, vibration damping, and enhanced energy absorption. As these reinforced polymeric materials are viscoelastic in principle, the mechanical behavior was characterized under two extremes of strain rate loading. In this article, the macroscopic response of brominated vinyl ester reinforced with 1.25 and 2.5 wt % nanoclay and exfoliated graphite platelet is considered. Air-blast experiment was conducted by subjecting these specimens to a high-transient pressure in a shock-tube with flexural loading configuration. The axial response was investigated quasi-statically in a uniaxial tension/compression test and dynamically in a compression Split-Hopkinson bar test. The servo-hydraulic MTS system was used to simulate the shock-tube testing in a flexural quasi-static loading configuration. High strain rate properties obtained from shock-tube experiment are compared with that of characterized under the simulated quasi-static flexural loading. Further, a computational finite element analysis model was developed in ANSYS LSDYNA to predict with reasonable accuracy the dynamic response of shock-loaded nanoreinforced specimens. Drop in both failure strain and energy absorption was observed with the addition of nanoparticles to pristine vinyl ester. However, an improvement in energy absorption was observed in case of shock-tube loading at high strain rates as compared to that loaded quasi-statically. © 2012 Wiley Periodicals, Inc. J Appl Polym Sci 000: 000–000, 2012

Key words: nanocomposites; reinforcement; clay

INTRODUCTION

Traditional composite materials are no longer capable of satisfying rigorous requirements for materials with enhanced mechanical and thermal properties, nor can they be engineered to control properties at the atomic scale. The essence of such control in properties has derived from the fact that the bulk properties of materials under external loading such as impact pressure or temperature are largely dictated by their molecular level orientation. Eventually, nanocomposite systems could be built at the molecular level to create large structures with primarily new molecular organizations.

What makes nanocomposites attractive is the extremely great interaction between small-scale particles and the matrix resin within the nanostructure. An interphase of 1-nm thick represents about 30% of the total volume in case of nanocomposites where as it reaches to 0.3% of the total volume of polymer in case of microparticle-filled composites.[1] The large interfaces within the nanostructure also enhance adhesion energy which translates into increase molecular bonding, and this increase in chemical bonding develops the polymer crosslinking and improves both mechanical and thermal properties. Conversely, a negligible contribution made by the interphase provides diverse possibilities of performance tailoring and is able to influence the properties of the matrices to a much greater extent under rather low nanofiller loading.

In addition to possessing extremely high mechanical properties (strength and modulus),[2] which are the apparent advantages for polymeric nanocomposites, nanotubes, for instance, are predicted to have an interesting mode of plastic behavior, that is experience a step-wise diameter reduction (local necking) and lattice orientation change.[3] Such highly bendable elastic stretching is extremely useful and could play an important role in increasing the toughness of nanotube-filled composites by increasing the energy absorbed during deformation. Significant improvement in the

Correspondence to: A. Almagableh (amalmag1@gmail.com).
Contract grant sponsor: Office of Naval Research, Solid Mechanics Program; contract grant number: N00014-07-1-1010.

tensile properties of polypropylene composites has also been reported in terms of stiffening, strengthening, and toughening with a low-filled content of about 0.5%.[4]

Scope of this investigation is to study this class of nanocomposite system against blast loading applications. Applications involve marine composite structures; particularly, lightweight glass/carbon polymeric-based composites, and innovative concepts for the mitigation of blast/shock/impact effects. Sandwich composites with balsa and foam cores are presently being featured in the number of navy applications such as in surface ship deck structures, radar mast, and boat hulls. Several new and emerging cores have been explored in sandwich construction. Different core types have been considered including Tycor (TYCOR® from Webcore Technologies) is an engineered three-dimensional fiber reinforced damage tolerant core for sandwich structures and has the potential to provide improved blast and ballistic resistance. This article presents our recent results on processing of brominated vinyl ester structural composites with nanoreinforcement for marine composite applications. Instead of using the commercial Derakane 411-350 vinyl ester resin, a 510A-40 brominated bisphenol-A-based vinyl ester consisting of 38 wt % styrene was developed and modified to produce the maximum degree of fire retardancy combined with enhanced chemical resistance and toughness. These brominated 510A-40 vinyl ester resin systems are planned to be used in the composite face sheets of sandwich structures with fire-resistant foam layered in between to further reduce flammability along with optimal flexural rigidity, vibration damping, and enhanced energy absorption.

Bromination of vinyl ester resin was found to exhibit good corrosion resistance, toughness, and imparts retardancy of fire, smoke, and toxicity which are of significant concern in ship structures.[5]

Effects of bromination on the viscoelastic properties of Derakane vinyl ester reinforced with 1.25 and 2.5 wt % nanoclay and graphite nanoplatelets were investigated using DMA.[6] Frequency sweep across three decades: 0.01, 0.1, 1, and 10 Hz was performed over temperature range from 30 to 150°C at a step rate of 4°C/min. The time–temperature superposition principle was applied to create master curves of dynamic storage modulus at a reference temperature. Results revealed drop in initial storage modulus with bromination for all the tested specimens; however, pure vinyl ester and nanocomposites with bromination exhibited higher glass transition temperature and damping (Tan $_{\delta}$ peak).

Bromination outcome on punch shear characteristics for laminated face sheets and sandwich composites of vinyl ester nanocomposites was investigated using Dynatup 8250 drop-weight impact instrument.[7] Test results showed that more than 10% improvement in impact energy absorption with addition of 2.5 wt % graphite platelets to brominated resin.

Understanding the panel response to shock loads, and developing accurate mechanical models will help in establishing future design criteria. In this article, the shock response of brominated 510 A-40 vinyl ester with 1.25 and 2.5 wt% nanoclay and graphite platelet is studied. The Split-Hopkinson bar, shock-tube, and the servo-hydraulic Material Testing System were used to characterize the mechanical response of these nanocomposites. A computational efficient FEA model is developed to predict the shock response of these nanoreinforced specimens. Further, the FEA approach was implemented to validate the conducted experiments.

EXPERIMENTAL

Materials and sample preparation

The matrix used here is a DERAKANE 510A-40 vinyl ester resin (manufactured and supplied by Ashland specialty chemical, Division of Ashland INC, Columbus, OH). This DERAKANE 510A-40 vinyl ester resin is a brominated bisphenol-A-based vinyl ester consisting of 38 wt % styrene, and modified to produce the maximum degree of fire retardancy combined with enhanced chemical resistance and toughness. These additives are butanone peroxide, *N*,*N*-dimethylaniline, cobalt naphthenate, and 2,4-pentanedione, all supplied from Sigma Aldrich, St. Louis, MO.

Exfoliated graphite nanoplatelets (xGnP) were produced at Michigan State University according to the method described in Ref. [8] The nanoclay was Cloisite 30B from Southern Clay Products, Gonzales, TX. The xGnP nanocomposites have exfoliated and dispersed graphite platelets with 1-nm thickness and several hundred nanometers widths. Distance between layers is in the range of 10–30 Å and size of the layered graphite extends from several hundred nanometers to several microns. Figure 1(a,b) shows morphology using TEM and SEM for xGnP inside the matrix and Figure 1(c) shows nanoclay dispersion.

Specimens were prepared by dispersing about 6.6 lbs of epoxy vinyl ester resin solution with different percentages of nanoclay/nanographite in a 1-gal container for 4 h, followed by four passes through a flow cell connected to a 100-W sonicator. In brief, 1% butanone peroxide, 0.2% of 2,4-pentanedione, 0.1% *N*,*N*-dimethylaniline, and 0.2% cobalt naphthenate were added to the mixed vinyl ester resin solution in order and mixed for 10 min. The above

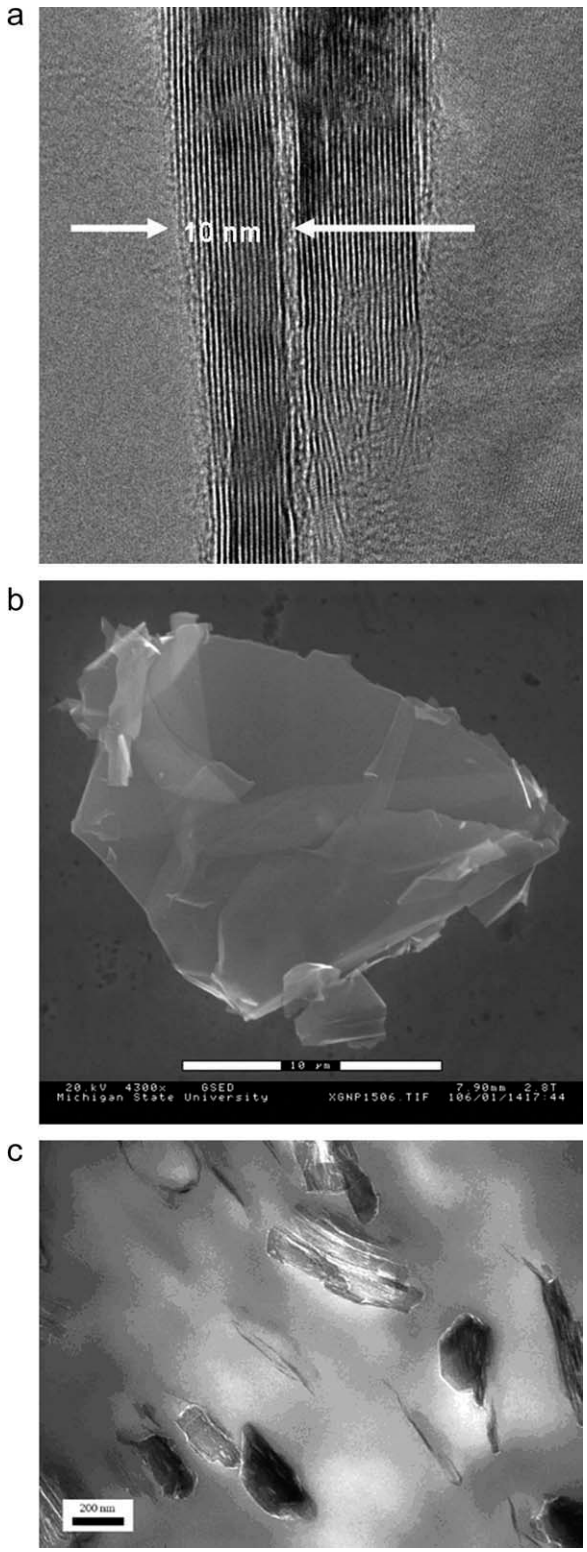

Figure 1 Morphology of nanoparticles dispersion (a) edge view (TEM) of xGnP, (b) lateral view (SEM) of xGnP, and (c) Cloisite® nanoclay.[14]

mixed resin solution was mixed for 2 min with FlackTek speed mixer at 3000 rpm. The well-mixed vinyl ester resin solution with nanoclay/nanographite was poured into a 13" × 13" × 0.4" mold, let stand for 30 min at room temperature, and then was postcured at 80°C for 3 h.

Quasi-static axial test

Tensile Quasi-static tests on 10-in long specimens were carried out on the Material test system Model 3180 (MTS System, Minnesota, MN) operating at a cross-head speed of 0.05 in/min (corresponding to a strain rate of 0.001/s). Tests were carried out according to ASTM D 638-08 ASTM.[9] An extensometer was employed to measure plastic deformation, and lubricant was applied between the specimen and the loading platens to reduce friction.

Compressive tests on another set of 5.5-in specimens were performed on same machine operating at similar crosshead speed as in tensile test. The compressive force was introduced to the specimen by a typical combined loading compression test fixture according to ASTM D 6641.[10] A strain gauge was attached to the specimen in the compression test setup to measure axial deformation up to 3% strain from which the compressive modulus was estimated.

Hopkinson bar tests

Split-Hopkinson Pressure Bar (SHPB) is utilized in the high-strain-rate testing of these nanomaterials at a strain rate of 1500/s. The pressure bar consists of a striker bar, an incident bar, and a transmission bar made of steel. Schematic diagram of the SHPB is shown in Figure 2.

A 0.5-in diameter testing specimen is placed between the incident bar and the transmission bar. When the striker bar impacts the incident bar, an elastic compressive stress pulse (shock wave), referred to as the incident wave, is generated and travels along the incident bar toward the specimen. The pulse duration equals the round-trip time of longitudinal elastic bar-wave in the striker bar. When the incident wave reaches the specimen, part of the pulse is reflected back in the incident bar owing to impedance mismatch at the bar/specimen interface, and the outstanding is transmitted through the specimen into the transmission bar.

Strain gages are mounted on the bars; provide time measures of the pulses in the incident and the transmission bars. Dynamic stress–strain and strain rate are calculated based on a one-dimensional elastic bar-wave theory for pulse propagation using Lagrangian diagram.[11]

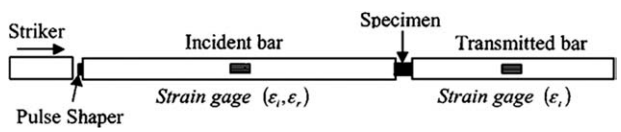

Figure 2 Schematic of Split-Hopkinson pressure bar.

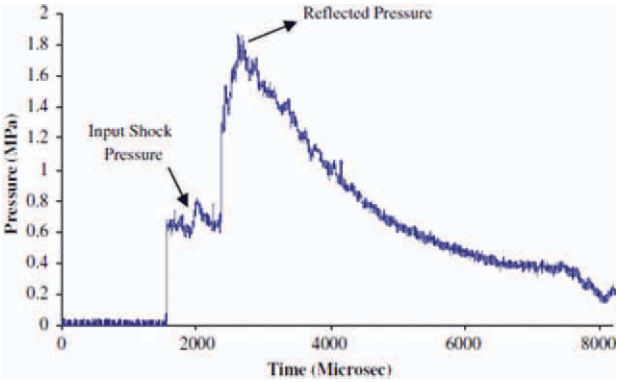

Figure 3 Typical shock pressure profile obtained in shock tube. [Color figure can be viewed in the online issue, which is available at wileyonlinelibrary.com.]

Air blast loading

A shock tube typically consists of high-pressure (driver) and low-pressure (driven) sections separated by a diaphragm. The driver and driven sections have a 6-in inner diameter and the converging section begins as 6-in diameter and ends 3 in. The tube is operated by pressurizing the high pressure section until the pressure difference across the diaphragm reaches a critical value and it ruptures. This rapid release of gas creates a shock wave that propagates down the tube to impart air blast loading on a specimen.

The shock-loaded brominated nanoreinforced panels were rectangular plates of 10-in long, (4-in wide and 0.39-in thickness). These plates were held under simply supported boundary conditions so as to minimize damage owing to gripping and clamping. The span of the simply supported plate was 6 in, and the overhangs measured 2 in along each end. The center of the specimen was kept in line with the center of the shock tube and the ratio of the loading diameter to the span was 0.5. The specimens were blast loaded from the muzzle of the shock tube on the face opposite to the supports.

The shock tube is instrumented with pressure and velocity measurements to provide real-time data about the shock pressure and shock velocity. A PCB 134A23 dynamic pressure sensor is mounted at the muzzle section of the shock tube and graphite rods are used to measure the shock velocity.

A typical pressure history obtained from shock tube is shown in Figure 3. The first peak pressures obtained in such experiments are called as "input shock pressure." The second peak is the "reflected shock pressure" from the specimen that the shock blast is impinged upon.

Flexural quasi-static test

The Material Test System machine operating at a crosshead speed of 0.05 in/min (corresponding to a strain rate of 0.001/s) was again used to evaluate the material response under flexural loading with similar boundary and loading configuration as in shock tube experiment. Specimen dimensions and span length of the simply supported conditions were kept similar to shock tube experiment. Quasi-static experiments were conducted under flexural deformation loading using a three-point bending fixture. A 3-in diameter steel cylinder was attached to the load cell through a threaded stud, creating a circular loading configuration (match the shock pressure). The steel cylinder is then embedded inside a bag filled partially with sand in the bottom to simulate uniform pressure distribution up to failure of the specimen. Figure 4(a,b) shows this experimental setup in the MTS system, with and without the sand-bag attached. Loading conditions in Figure 4(b) simulate distributed loading conditions (similar to shock tube test), whereas the load in Figure 4(a) simulates a four-point loading configuration.

A *C*-clamp fixture was used to mount two external linear variable-differential transformers (LVDTs) at the middle on both sides of the specimen to capture midspan deflection and connected via a strain

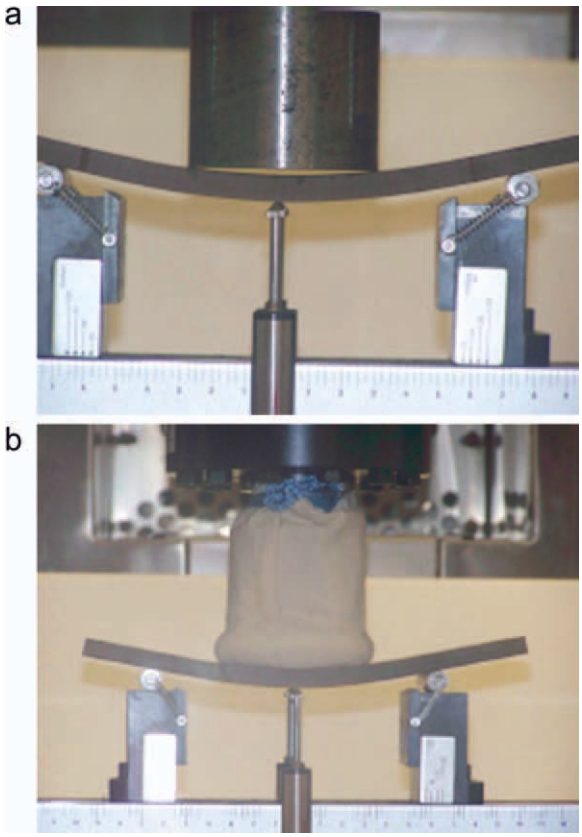

Figure 4 Quasi-static loading of nanoreinforced specimen, (a) without a sand bag, and (b) with the sand bag (to simulate distributed shock tube pressure loading). [Color figure can be viewed in the online issue, which is available at wileyonlinelibrary.com.]

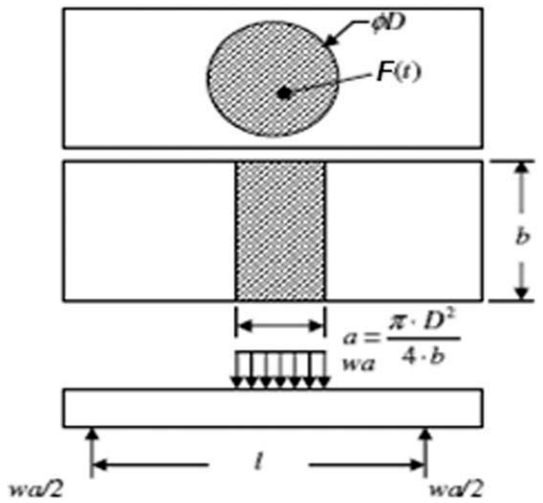

Figure 5 Boundary conditions for shock and flexural quasi-static tests..[12]

indicator box. Load and stroke displacement were obtained from the load cell and actuator movement. It should be noted that the midspan deflection (measured by LVDTs) was not the same as the stroke displacement of the system crosshead, and the two data sets have been synchronized independently over time.

Strain rate analysis

An approximation of the strain rate under quasi-static flexural loading is computed[12] using bending moment analysis to assess numerical work. The quasi-static flexural strain, $\varepsilon(t)$ can be obtained from Hooks law as:

$$\varepsilon(t) = \frac{M\,y}{E\,I} \tag{1}$$

where E and I are young modulus and area moment of inertia, respectively, and y is the distance from the neutral axis. The induced bending moment, $M(t)$, was computed from the load time history obtained at each time step (t). The load (F) applied on the circular region was approximated as a distributed loading, w, (Newton/meter) acting on a rectangular area along the beam width of length, a, and width, b, as shown in Figure 5.

With this approximation, the maximum bending moment at the midspan is given by:

$$M(t) = \frac{1}{8}F\,(2l - a) \tag{2}$$

Substituting the values of $M(t)$, y and I into eq. (1), $\varepsilon(t)$ is given as:

$$\varepsilon(t) = \frac{1}{8}\frac{F(t)\,(2l - a)\,(d/2)}{E\,(bd^3/12)} \tag{3}$$

where d is the beam thickness. The strain versus time evaluated as a function of the load history, $F(t)$, was plotted using eq. (3) for both the quasi-static flexural and the shock loading. The only difference is that the pressure data obtained as an output from shock have been converted into force by multiplying with the effective area. It should be noted that this is only an approximation as the Young modulus (E) obtained from quasi-static tensile testing was used in eq. (3) for obtaining transient strain history.

A graph showing the computed strain versus time for brominated vinyl ester under quasi-static and shock loading is shown in Figures 6 and 7, respectively. Vinyl ester specimen was observed to posses relativley higher strain over longer duration of time under quasi-static loading. As per this approach, the

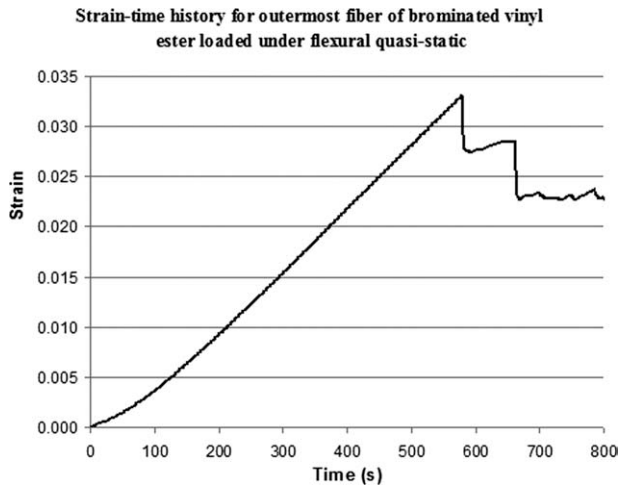

Figure 6 Transient strain history for the outermost fiber of brominated vinyl ester, loaded under flexural quasi-static test.

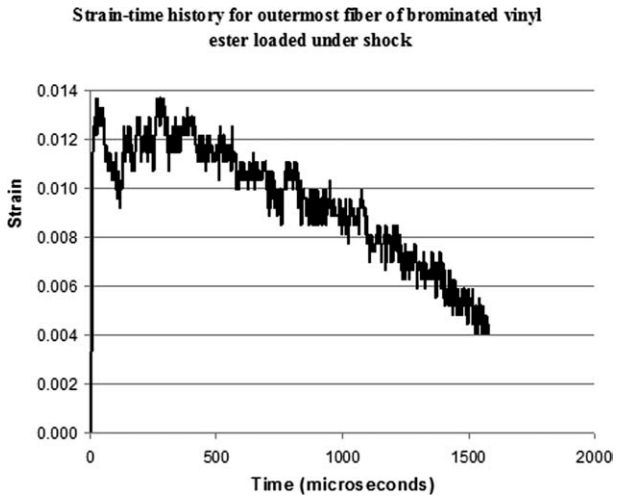

Figure 7 Transient strain history for the outermost fiber of brominated vinyl ester, loaded under shock.

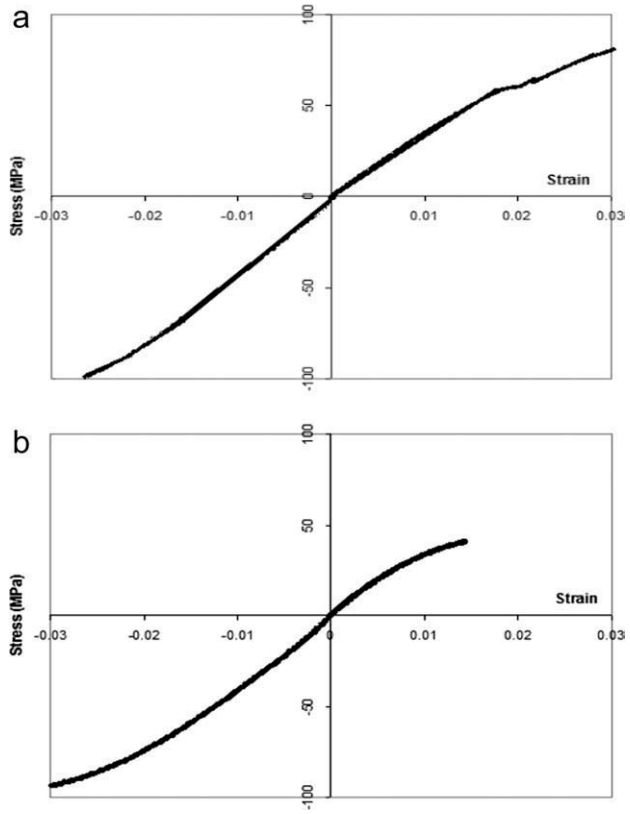

Figure 8 Tension and compression stress–strain data for (a) brominated vinyl ester, and (b) brominated vinyl ester with 2.5 wt % xGnP.

strain rates computed for quasi-static and shock loading were 0.0001 and 1000/s, respectively.

EXPERIMENTAL RESULTS

In general, failure mechanism of nanoreinforced composites is more complicated than common fiber/laminate composites. This is because the fact that the distribution of nanoparticles in the matrix can be either random or in preferred orientations, and thus the stress distribution within the nanostructure can be extremely complex.

For a viscoelastic material, rate of loading is a fundamental characteristic, as energy absorption up to failure may vary for different strain rates. Therefore, the mechanical response and energy absorption characteristics under different strain rate loading were considered.

Quasi-static tension and compression

Typical stress–strain curves for both tension and compression of some nanocomposite specimens are shown in Figure 8. In fact, the system with 2.5% xGnP infusion has both the lowest strength and the lowest failure strain [Fig. 8(b)] but stable stiffness among the two systems was observed. That was not surprising much owing to the fact that the previous studies with nanoparticle[13] did not show such improvement.

Possible reasons for drop in failure strain could be that the xGnP reinforcement did not contribute much to the elongation, and that the failure was mostly controlled by nucleation of cracks (inclusions) which are the predominant forms of damage during failure under quasi-static loading. These cracks begin to nucleate either at inhomogeneities such as nanoparticle sites and interact with defects (pores) within the resin neat creating a larger crack area with more energy dissipated.

Shock loading

Theory of shock wave propagation indicates that rupture occurs when successive shock waves meet after multiple reflections over an interface (nanoparticles), which results in what so-called spalling. The deflection history of the shock-loaded nanocomposite samples was captured in frames of 150 microsecond time duration as shown in Figure 9. The shock loading is observed to induce maximum deflection at the center of the panels and reduced gradually toward the end.

Viscoelastic material is typically become stiff when subjected to high strain rate loading. This is typically observed in most of the nanoreinforced systems. Increase in stiffness at high strain rate was also dictated from stress–strain curves obtained using the SHPB. The stiffer material can lead to a lower deflection which in turn shows lesser energy absorption.

Energy absorption

The energy absorbed by vinyl ester nanocomposites obtained from numerical integration of the load versus midpoint deflection is shown in Figure 10. Energy absorption is studied at different strain rates by comparing behavior of nanocomposites in case of shock with those simulated flexurally in MTS. As mentioned before, loading configuration (distributed pressure profile) was kept the same in both experiments. All specimens loaded quasi-statically were observed to have less mid-deflection as compared to those tested in shock. For example, specimens with xGnP showed an increase in energy absorption up to 150% in shock as compared to quasi-static. Conversely, in case of both shock and quasi-static loading, addition of either nanoparticles (nanoclay and xGnP) to brominated resin resulted in drop in failure strain and energy absorption capability.

In case of shock loading, energy behavior varies from nanocomposite system to another based on type and amount (wt %) of nanoparticle used. For example, comparing the central deflection in Figure 10,

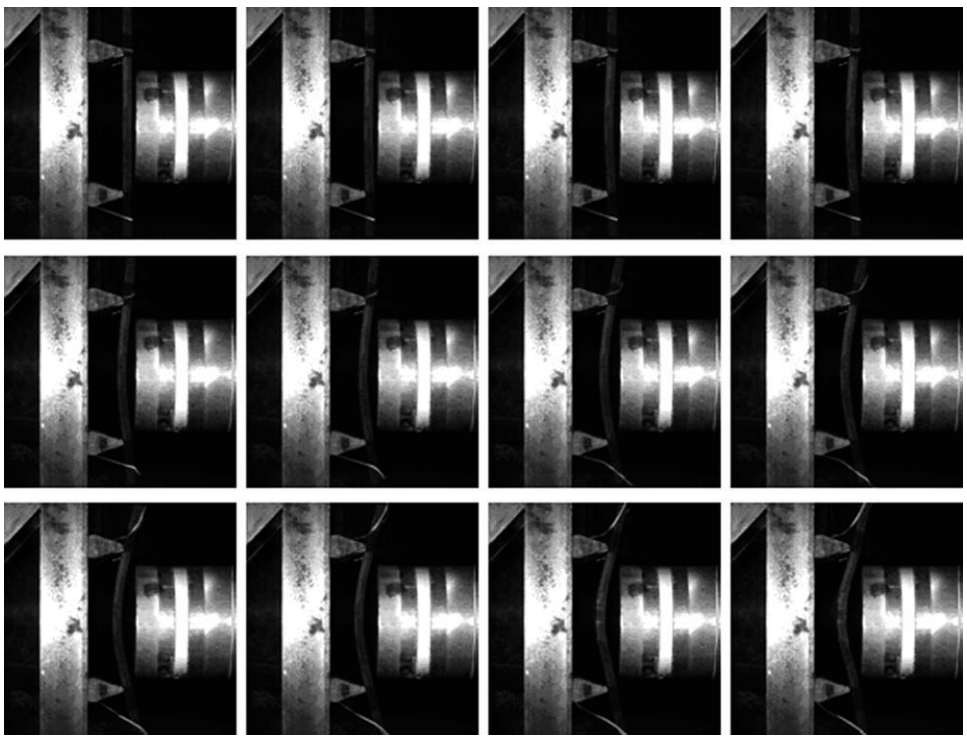

Figure 9 Typical real time images for vinyl ester under shock loading.

nanoclay system exhibited greater deflection as compared to xGnP of the same weight loading (black bars). In contrast, the energy behavior is about the same for both systems with 2.5 wt % nanoclay and 2.5 wt % xGnP as shown in Figure 11. This phenomenon can be owing to some error/uncertainty in processing energy absorption out from force–deflection data set for the two experiments.

To sum up, addition of nanoparticles of either xGnP or nanoclay to brominated resin did not show such improvement in deflection and energy absorption quantities. Moreover, tremendous drop in mechanical properties (energy absorption) is more pronounced with adding xGnP rather than that associated with nanoclay reinforcement. On the contrary, another study reported 10% improvement in impact energy absorption with addition of 2.5 wt % graphite platelets to brominated resin.[7]

Finite element approach

Finite element modeling of brominated vinyl ester nanocomposite beam specimens subjected to both

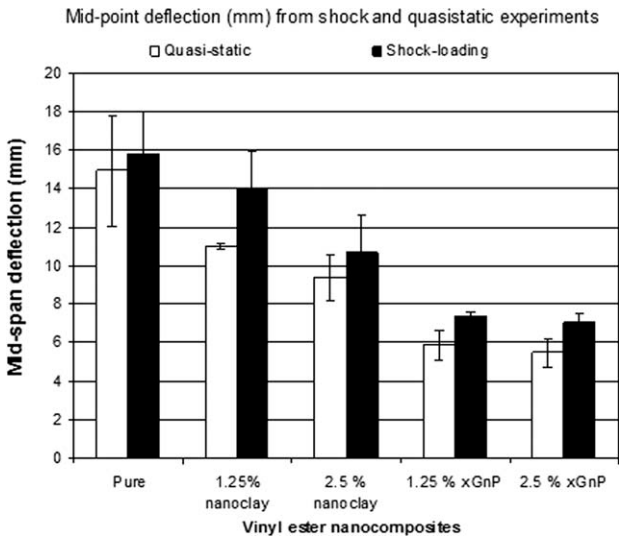

Figure 10 Midpoint deflection at failure under both quasi-static flexural and shock experiments.

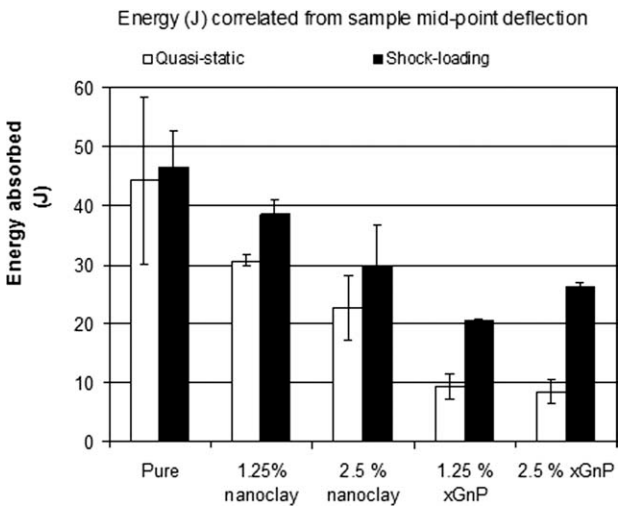

Figure 11 Energy absorption characteristics for both quasi-static flexural and shock experiments.

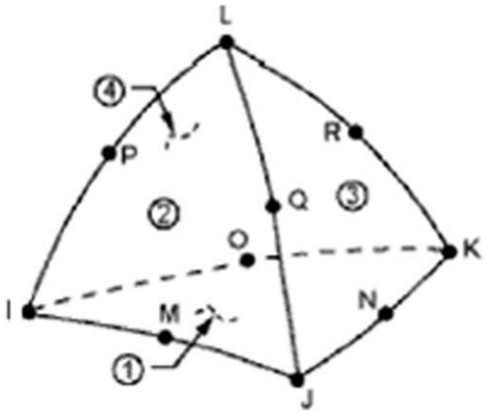

Figure 12 Solid 168 element geometry.

shock and quasi-static flexural loading was attempted in this study. The nanocomposite materials are considered isotropic because the nanoparticles are randomly dispersed in the vinyl ester matrix. ANSYS LS-DYNA with explicit analysis was used to predict the dynamic response of the shock-loaded materials, whereas ANSYS was applied for modeling the quasi-static flexural experiment. Solid 168, a higher order 3D, 10 node tetrahedral structural solid explicit dynamic element was used for modeling (Fig. 12).

Modeling of the beam structure was established by connecting appropriate key points in the same way as in shock tube setup. A refined mesh in the loading area (circular) and a course one in the outer regions were applied. As the specimen was held under a simply supported boundary condition with a 6-in span length, the respective lines in the model were restrained to move in the (loading) z-direction. Also, the center (origin) node on the specimen and the center of the left support were restrained to move in xy-plane to avoid twisting mechanism as shown in Figure 13. Deformed shape of the structure owing to load applications under both experiments with midpoint deflection was captured from the finite element simulations.

Shock tube analysis

A nodal load was applied in the shock experiments on all nodes of the circular region owing to the inherent problems in applying area load in a 3D element under explicit ANSYS-LSDYNA analysis. Load on the nodes on periphery of the circle (external nodes) was half in magnitude to that on nodes inside the circular region (internal nodes). There were totally 4965 internal nodes and 240 external nodes on the loading area of which the FEA solution stabilized. Load was applied with the discreet values obtained from the pressure profile curve and was divided in 5085 (4965 + 240/2) equal parts. Load was applied in the form of two arrays with one row containing time data and the other row containing the respective load values. Two more arrays were generated, one for internal nodes and one for external nodes. Time at which maximum deflection was observed in shock experiments has been defined as the time at end of the load step.

Two different material models have been applied in FEA to simulate the shock response of these nanocomposites. The first material model used was the standard piecewise material model. This model provides a multilinear elastic–plastic material behavior that allows stress versus strain curve and strain rate dependency. Engineering stress–strain and failure strain were obtained from high strain data (Hopkinson bar) and converted to true stress-true plastic strain, defined as a material input. The failure criterion is defined by the effective failure plastic strain.

The linear viscoelastic material model introduced by Herrmann and Peterson was applied in the FEA analysis of shock tube loading. This principle asserts that the total strain (stress) resulting from the application of a sequence of stresses (strains) is equals to the sum of strains (stresses) caused by individual stresses (strains). To define a linearly viscoelastic constitutive model in FEA, the experimental stress relaxation data obtained from DMA tests over a wide range of temperatures were shifted to a room temperature, and then fitted into eq. (4) as shown in Figure 14. According to this model, the parameters G_∞ (relaxation modulus at ∞ time), G_o (initial relaxation modulus), K (bulk modulus), and the constant, β, are required to define the linear viscoelastic model in ANSYS LSDYNA.

$$\phi(t) = G_\infty + (G_o - G_\infty)e^{-\beta t} \tag{4}$$

The elastic bulk behavior is assumed when calculating the incrementally integrated pressure (P) from

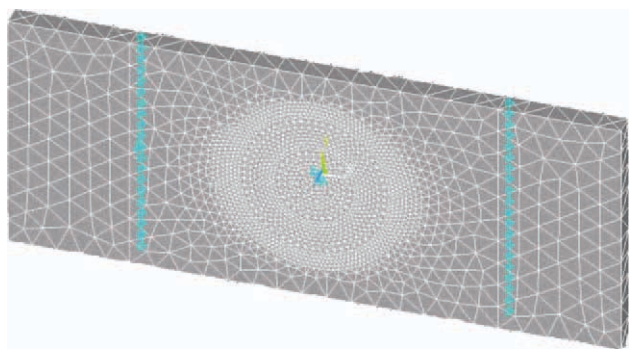

Figure 13 Finite element model of shock tube experiment with boundary conditions. [Color figure can be viewed in the online issue, which is available at wileyonlinelibrary.com.]

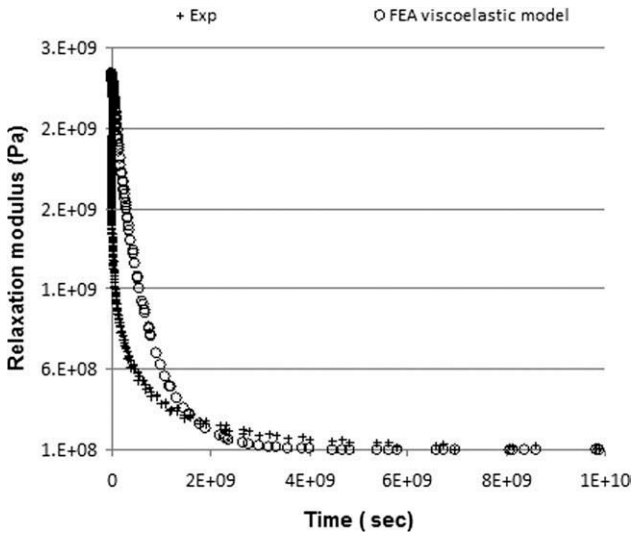

Figure 14 Shear relaxation modulus for vinyl ester as function of time from DMA.

volume (v). Thus, the total stress calculated based on the linear viscoelastic model is given as:

$$\sigma_{ij} = 2\int_0^t \phi(t-\tau)\left[\frac{\partial \varepsilon_{ij}(\tau)}{\partial \tau}\right] d\tau + (K \ln v)\delta_{ij} \qquad (5)$$

Following maps as in the previous analysis (Fig. 7), a transient strain history of the outmost fiber for vinyl ester modeled under shock is shown in Figure 15. FEA results in terms of the maximum strain and strain rate of the outermost fiber do agree well with that obtained experimentally as per the linear bending approach (Fig. 7).

Figure 16 shows the deformation of pure vinyl ester subjected to 120 psi peak pressure obtained from finite element modeling.

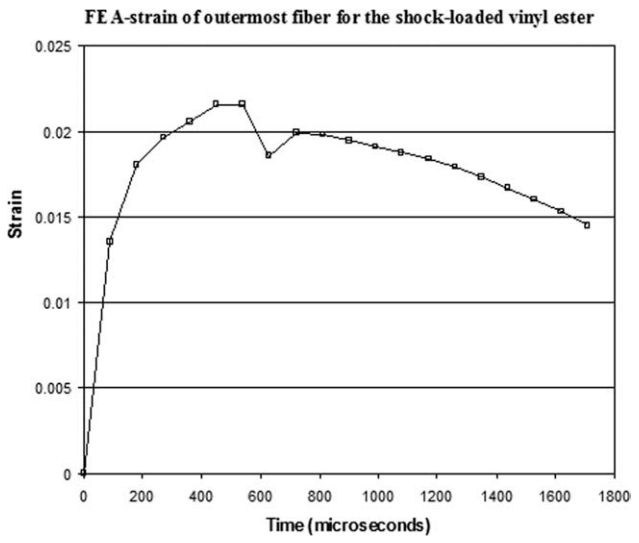

Figure 15 FEA strain of outermost fiber for the vinyl ester specimen under shock.

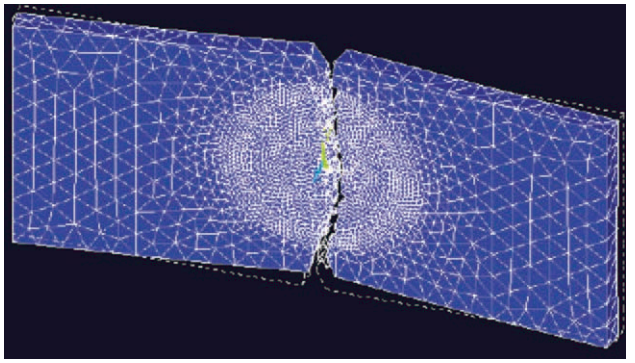

Figure 16 Deformation of pure vinyl ester subjected to 120 psi pressure in a shock tube. [Color figure can be viewed in the online issue, which is available at wileyonlinelibrary.com.]

Figures 17 and 18 show midpoint deflection (outermost fiber) at failure for brominated vinyl ester with nanoclay and graphite platelet nanoreinforcements, subjected to 120 psi peak pressure and also the predictions obtained from finite element analysis using both piecewise linear (high strain rates data) and viscoelastic response as input parameters. It is observed that the viscoelastic model gives a marginally better prediction of sample midpoint deflection compared to the piecewise (high strain rate) linear material models. The time–temperature superposition principle applied in shifting the viscoelastic property used in FEA-LSDYNA is based on the fact that processes involved in molecular motion occur at larger rates at elevated temperatures. Thus, these materials proved to react in a linearly viscoelastic behavior although subjected to a high strain rate loading (shock) over microseconds. That is to say, the short time duration of the shock pulse imposed

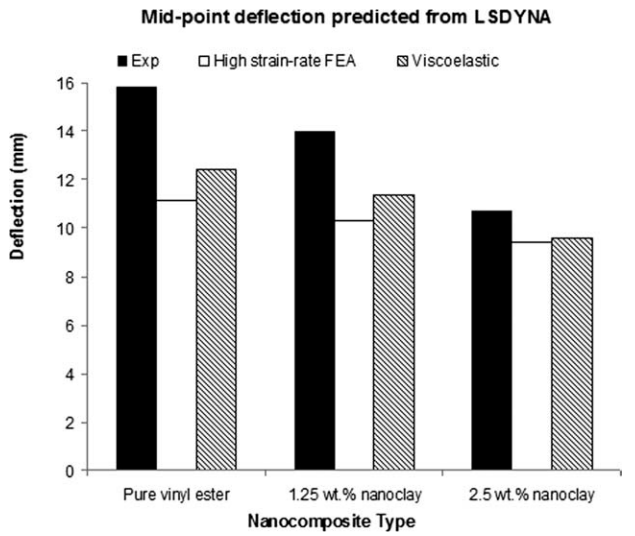

Figure 17 FEA predictive and experimental midpoint deflection for nanoclay reinforced vinyl ester.

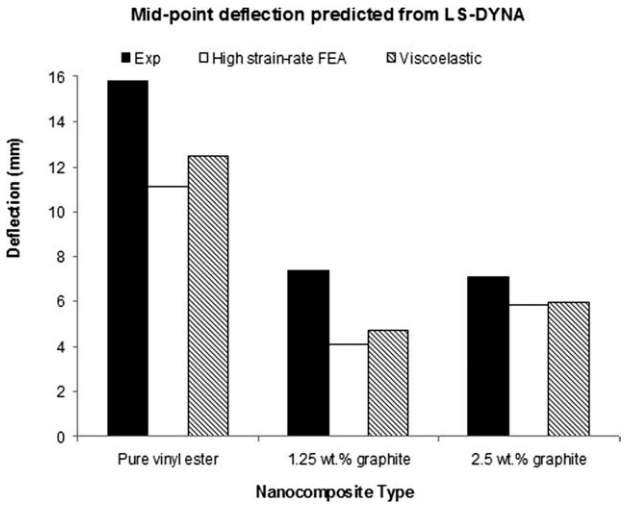

Figure 18 FEA predictive and experimental midpoint deflection for graphite reinforced vinyl ester.

on the viscoelastic material is theoretically compensated by the time–temperature superposition which accelerates molecular motion as if occurs at elevated temperatures and elevated strain rate.

Quasi-static flexural analysis

The quasi-static flexural experiments (with sand-bag) conducted on a given nanocomposite sample in the MTS test system were modeled and validated in ANSYS. The element type, model geometry, boundary conditions, and loading configuration are kept exactly similar to those used for simulating the shock tube response. Both the tension and the compression engineering stress–strain data were defined as constitutive material models under the nonlinear with large deformation analysis method. The experimental maximum load from MTS was converted to a uniform pressure and applied in ANSYS in constant increments over a certain number of substeps. Failure model in ANSYS is based on Von Mises criterion which assumes that yielding will occur only when the second invariant of the deviatoric stress reaches a critical value (strength). Failure occurrence is dictated from postprocessing of Von Mises stress data, and cannot be directly dictated or shown from solution interface.

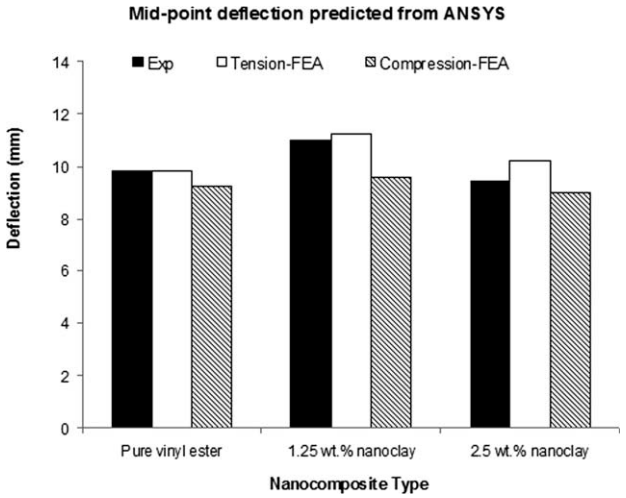

Figure 19 FEA predictive and experimental midpoint deflection for nanoclay/510A-40 vinyl ester under quasi-static flexural loading.

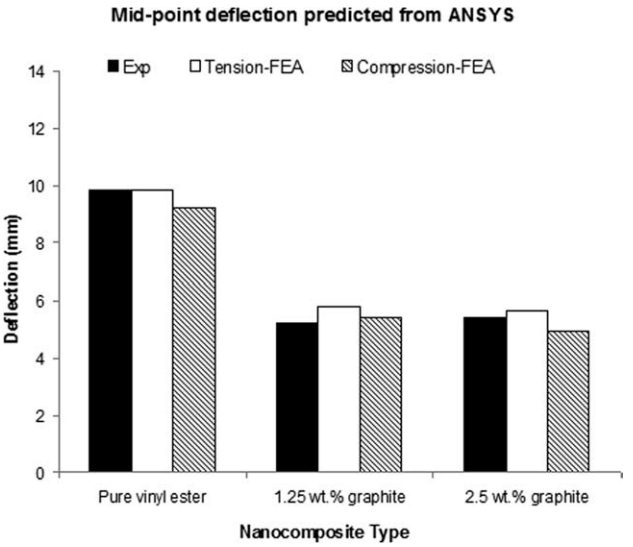

Figure 20 FEA predictive and experimental midpoint deflection for graphite platelet/510A-40 vinyl ester under quasi-static flexural loading.

FEA midpoint deflection results for the nanocomposites loaded under quasi-static (with the sand-bag) are shown in Figures 19 and 20. It should be noted that tension and compression data obtained from the two independent quasi-static tests (described earlier) were used for defining the material constitutive models. From ANSYS results, the quasi-static flexural experiment conducted with the sand bag to simulate the distributed shock pressure was modeled and validated.

CONCLUSIONS

Brominated vinyl ester nanocomposite systems are viscoelastic materials in basis which are sensitive to the rate of loading applied, time, and temperature dependent as well. Therefore, the mechanical response had been investigated over two extremes of strain rates loading. The high strain rate response of nanoclay and graphite platelet reinforced 510A-40 vinyl ester was first studied by conducting air blast loading using the shock tube. On the other extreme, the servo-hydraulic MTS test system was used to study the material behavior under quasi-static loading, with boundary conditions and loading configuration similar to shock tube experiments.

Experimental results showed that addition of nanoparticles to brominated resin adversely affected the energy absorption capability under shock loading. These nanoreinforced materials become stiffer and exhibited drop in failure strain when subjected to shock. Moreover, this increase in stiffness under shock was also dictated from stress–strain curves obtained using the Hopkinson bar. On comparing the loading rate, all the nanosystems tested were observed to absorb greater energy under high strain rate (shock) as compared to the quasi-static flexural mode.

Lesser energy absorbed within the low strain rate as compared to shock loading could be owing to role of nanoparticles toward failure. Cracks under quasi-static may begin to grow over the nanoparticles sites (inclusions), and then these small size cracks interact with pores within the vinyl ester matrix making larger cracks with larger stress concentrations. On the other hand, failure mechanism of nanoreinforced specimens under shock loading could be owing to complex shock wave propagation.

Finite element modeling of the shock tube loading showed that the linear viscoelastic model gives marginally better prediction of sample midpoint deflection compared to the high strain rate piecewise linear material model. As a result, these materials proved to react in a linearly viscoelastic behavior although subjected to a high strain loading (shock) over microseconds. The short time duration of the shock pulse imposed on the viscoelastic material is theoretically compensated by the time–temperature superposition which accelerates molecular motion as if occurs at elevated temperatures and elevated strain rate. The quasi-static flexural experiment conducted with the sand bag to simulate the distributed shock pressure was modeled and validated in ANSYS.

The nanoclay and graphite platelet vinyl ester composite panels were manufactured by Dr. Lawrence T. Drzal's group at Michigan State University.

References

1. Kojima, Y.; Fukimori, K.; Usuki, A.; Okada, A.; Karauchi, T. J Mater Sci Lett 1993, 12, 889.
2. Xu, X.; Thwe, M.; Shearwood, C; Liao, K. J Appl Phys Lett 2002, 81, 2833.
3. Dresselhaus, M. S.; Dresselhaus, G.; Avouris, P. Carbon Nanotubes, Synthesis, Structure, Properties, and Application; Springer: New York, 2001.
4. LeBaron, P. C.; Wang, Z; Pinnavaia, T. J. J Appl Clay Sci 1999, 15, 11.
5. Sorathia, U.; Ness, J.; Blum, M. J Comp A: Appl Sci Manuf 1999, 30, 707.
6. Almagableh, A.; Mantena, P. R.; Alostaz, A.; Liu, W; Drzal, L. T. J eXPRESS Polym Lett 2009, 3, 724.
7. Pramanik, B; Mantena, P. R. J ASME Early Career Tech 2010, 8, 1.
8. Kalaitzidou, K.; Fukushima, H.; Askeland, P.; Drzal, L. T. J Mater Sci 2008, 43, 2895.
9. Laboratory of Polymer Technology-Polymer Blends, Available at: http://polymeeri.tkk.fi, 1/21/ 2010.
10. ASTM Standard D 638–08. Standard Test Method for Tensile Properties of Plastics; ASTM International: West Conshohocken, PA, 2008.
11. ASTM Standard D 6641/D 6641M. Standard Test Method for Determining the Compressive Properties of Polymeric Matrix Composite Laminates Using a Combined Loading Compression (CLC) Test Fixture; ASTM International, 2007.
12. Almagableh, A. Viscoelastic and shock response of nanoclay and graphite platelet reinforced vinyl ester nanocomposites, PhD Dissertation, 2010, Department of Mechanical Engineering, University of Mississippi.
13. Gupta, S. "Energy absorption characteristics of MWCNT/Nylon 6,6; and nanoclay and graphite platelet/vinyl ester nanocomposites", Master's Thesis. 2009, Department of Mechanical Engineering, University of Mississippi
14. Shiner, C.; Timmerman, J.; Ebonee, P. M.; Williams; Seferis, J. 48th International SAMPE Symposium, 2003, 2539.